

ALMA MATER STUDIORUM · UNIVERSITÀ DI
BOLOGNA

FACOLTÀ DI SCIENZE MATEMATICHE, FISICHE E NATURALI
Corso di Laurea in Fisica

**Construction of an empirical radar
data quality function and analysis of
its impact on radar data assimilation**

Laurea Specialistica in Fisica

Relatore:
Prof. Levizzani Vincenzo
Correlatore:
Dott. Rossa Andrea

Candidato:
Laudanna Del Guerra
Franco

Sessione II
Anno Accademico 2008-2009

Contents

1	Introduction	3
2	Data and methodology	5
2.1	Weather radar	5
2.1.1	Historical review	5
2.1.2	Physical review	7
2.1.3	Main error sources on radar measurements	8
2.1.4	Principal radar displays	11
2.2	The Veneto Radar network	12
2.3	The Swiss Radar network	13
2.4	The numerical model	14
2.5	Data assimilation: LHN	15
2.6	Data set	17
3	Derivation of an empirical radar data quality description	19
3.1	Analysis on frequencies of occurrence	19
3.2	Rest clutter identification	21
3.3	Quality function construction	23
3.4	Results	25
4	Assimilation experiments	29
4.1	Experimental setup and diagnostic material	29
4.2	Case descriptions	30
4.2.1	Mestre flood	30
4.2.2	Swiss cases	32
5	Results	35
5.1	Mestre case	35
5.1.1	Results on assimilation of radar data	35
5.1.2	Quality function results	40
5.2	Swiss case	42

CONTENTS **1**

6 Summary and discussion	45
6.1 Impact of radar data quality function	45
6.2 Impact of radar rainfall assimilation	47
Bibliography	49

Chapter 1

Introduction

In the last few years the resolution of numerical weather prediction (NWP) became higher and higher with the progresses of technology and knowledge. As a consequence, a a great number of initial data. The potential of radar observations has long been recognized for improving the initial conditions of high-resolution NWP models (Macpherson et al. [2004]), while operational application becomes more frequent.

Assimilation of data is a statistical discipline which aim to combine various bits of information, i.e. a short-term forecast and the most recent observations, given their relative quality (Kalnay [2003]). For this purpose we need to know, at all the grid points, the model error with all the covariances between the variables. In particular when we are using remote sense observation we should know the error covariance matrix. Keeler and Ellis [2000] derive an error covariance matrix using reflectivity, radial winds and spectrum width, while Berenguer and Zawadzki [2008] have proposed a physically based approach for the derivation of the radar covariance matrix for stratiform precipitation considering the effects of range and of the variability of the drop size distribution making use of disdrometer observations. Germann et al. [2006] derive an error climatology for precipitation estimates, while Sempere-Torres et al. [2008] propose a real time error estimation comparing precipitation estimates against a benchmark, i.e. two different stages of their quality control cascade.

Rossa and Michaelides [2005], Michelson et al. [2004] in the framework of COST 717 promoted significantly quality description of radar data and carried over to the EUMETNET OPERA program (Holleman et al. [2006]). Several approaches have been proposed based on how significant the quality control algorithms impact the observations (Friedrich and Hagen [2004], Fornasiero et al. [2006]).

All these efforts share a detaild knowledge of the radar systems as a

prerequisite to derive an error information. Some extra informations are often needed from complementary observations, such as disdrometers (Berenguer and Zawadzki [2008]) or a high-resolution rain gauge network (Germann et al. [2006]).

European countries have a very heterogeneous collection of national and even regional radar networks. The OPERA program (Operational Programme for the Exchange of weather RADar information) is making a significant effort to harmonize the radar data exchange but a standard for quality characterization has yet to be established. The fact that many NWP centres have recently taken into operations convection-permitting forecast models, many of which assimilate radar data, emphasizes the need for a pragmatic approach to providing quality information which is needed in order to avoid that radar errors degrade the model's initial conditions and, therefore, its forecasts (Rossa and Leuenberger [2008]).

Such pragmatic approaches have been widely applied and can be as simple as parametrizing the radar data quality with range (Jones and Macpherson [1997]). Geometrical visibility, or height above the surface of the lowest elevation of a pixel would be slightly more sophisticated but this visibility will depend on the atmospheric conditions and, therefore, on the season. (Germann and Joss [2004b]) show that a long-term precipitation accumulation reflects the radar visibility to some detail.

In this contribution a pragmatic and empirical approach to deriving a radar data quality description is proposed to be used in radar data assimilation and more specifically for the latent heat nudging (LHN) scheme. In section 2, after a review on radar the NWP, the latent heat nudging scheme and the cases are briefly described, while section 3 is devoted to the formulation of the quality function. In the next section will be described experiments executed and given a description of the meteorological events related to them. Results will be shown and discussed in section 5, and conclusions given in the final section.

Chapter 2

Data and methodology

2.1 Weather radar

2.1.1 Historical review

During World War II, military radar operators noticed noise in returned echoes due to weather elements like rain, snow, and sleet. Just after the war, military scientists returned to civilian life or continued their activity in the Armed Forces and pursued their work in developing a use for those echoes. In the United States, David Atlas, for the Air Force group at first, and later for MIT, developed the first operational weather radars. In Canada, J.S. Marshall and R.H. Douglas formed the "Stormy Weather Group" in Montreal. Marshall and his doctoral student Walter Palmer are well known for their work on the drop size distribution in mid-latitude rain that led to the understanding of the Z-R relation, which correlates a given radar reflectivity with the rate at which water is falling on the ground. In the United Kingdom, research continued to study the radar echo patterns and weather elements such as stratiform rain and convective clouds, and experiments were carried out to evaluate the potential of different wavelengths from 1 to 10 centimetres.

In 1953, Donald Staggs, an electrical engineer working for the Illinois State Water Survey, obtained the first recorded radar observation of a "hook echo" associated with a tornadic thunderstorm (2.1).

Between 1950 and 1980, reflectivity radars, which measure the position and the intensity of precipitation, were built by weather services around the world. The early meteorologists had to watch a cathode ray tube. During the 1970s, radars began to be standardized and organized into networks and the first devices to capture radar images were developed. The number of scanned angles was increased to get a three-dimensional view of the precipitation, so that horizontal cross-sections (CAPPI) and vertical ones could be

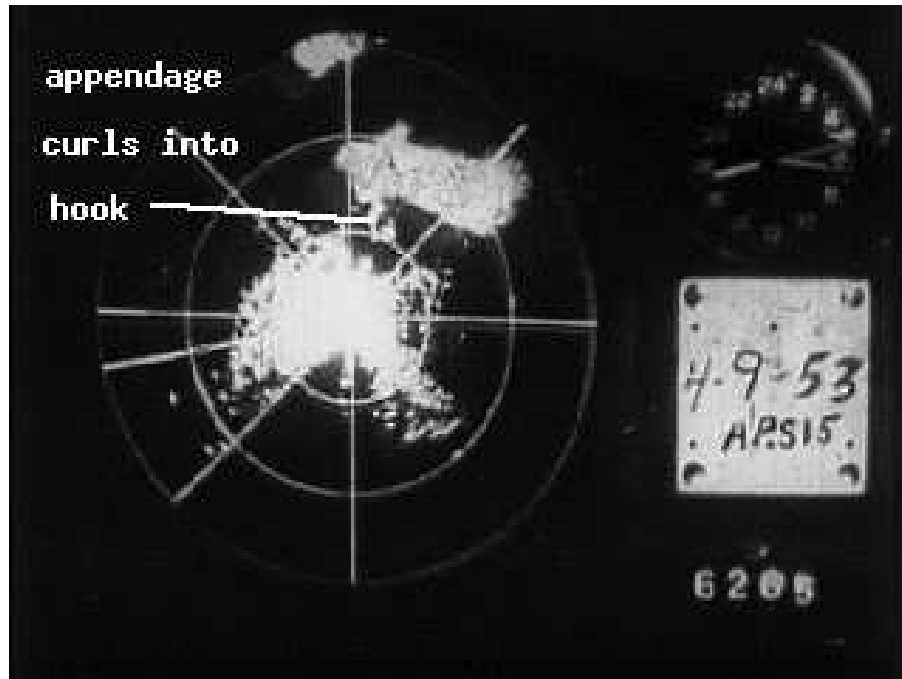


Figure 2.1: First radar image of an hook echo from the thunderstorm of 4/9/53 in Illinois

performed. Studies of the organization of thunderstorms were then possible for the Alberta Hail Project in Canada and in particular for National Severe Storms Laboratory (NSSL) in the USA.

The NSSL was started in 1964 and began experimentation on dual polarization signals and on Doppler effect. In May 1973, a tornado devastated Union City, Oklahoma, just west of Oklahoma City. For the first time, a Dopplerized 10-cm wavelength radar from NSSL documented the entire life cycle of the tornado. The researchers discovered a mesoscale rotation in the cloud aloft before the tornado touched the ground : the tornadic vortex signature. NSSL's research helped convince the National Weather Service that Doppler radar was a crucial forecasting tool. The Super Outbreak of tornadoes on April 3-4, 1974 and their devastating destruction might actually have been ok some help to get funding for further developments.

Between 1980 and 2000, weather radar networks became the norm in North America, Europe, Japan and other developed countries. Conventional radars were replaced by Doppler radars, which in addition to position and intensity of the air could track their relative velocity. In the United States, the construction of a network consisting of 10 cm wavelength radars, called NEXRAD or WSR-88D (Weather Service Radar 1988 Doppler), was started

in 1988 following NSSL's research.

In Canada, Environment Canada built the King City station, with a five centimeter research Doppler radar, by 1985; McGill University dopplerized its radar (J. S. Marshall Radar Observatory) in 1993. This led to a complete Canadian Doppler network between 1998 and 2004. France and other European countries switched to Doppler network by the end of the 1990s to early 2000s. Meanwhile, rapid advances in computer technology led to algorithms to detect signs of severe weather and a plethora of "products" for media outlets and researchers.

In Europe, from 1999, Opera Project work with objective to exchange expertise on operational radar issues and to harmonize and improve the operational exchange of wheather radar information between national meteorological services.

After 2000, research on dual polarization technology has moved into operational use, increasing the amount of information available on precipitation type (e.g. rain vs. snow). "Dual polarization" means that microwave radiation which is polarized both horizontally and vertically (with respect to the ground) is emitted. Wide-scale deployment is expected by the end of the decade in some countries such as the United States, France, and Canada.

2.1.2 Physical review

Weather radars send directional pulses of microwave radiation, on the order of a microsecond long. The wavelengths of 1 to 10 cm are approximately ten times the diameter of the droplets or ice particles of interest, because Rayleigh scattering occurs at these frequencies. This means that part of the energy of each pulse will bounce off these small particles, back in the direction of the radar station.

Shorter wavelengths are useful for smaller particles, but the signal is more quickly attenuated. In Europe 5 cm C-band system are preferred to 10 cm (S-band) radar because are less expensive, 3 cm X-band radar is used only for very short distance purposes, and 1 cm Ka-band weather radar is used only for research on small-particle phenomena such as drizzle and fog.

Weather radar equations resolution is are not of interest of for this thesis work, so, therefore only the final one is reproduced below:

$$P_r = \frac{\pi^3 c}{1024 \ln 2} \left[\frac{P_t G^2 \theta^2}{\lambda^2} \right] \left[|K|^2 \frac{Z}{r^2} \right]$$

Radar parameters are shown between the former square brackets, while target parameters are shown between the latter square brackets (see tab: 2.1 for further details on parameters).

Other two formulas are needed:
 Z definition and his relationship with P_r :

$$Z = \int_0^{\infty} N(D)D^6 dD$$

$$10 \log P_r = 10 \log Z - 20 \log r + C$$

Typically is used a Marshall and Palmer $Z - R$ relationship which is based on an esponential drop size distribution that produce:

$$Z = aR^b$$

were a and b are adjustable parameters that depends by precipitation type and site

Table 2.1: Parameters of radar power equation.

Parameter	Description
P_r	Radar power
P_t	Peak power
λ	wavelength
G	Gain
θ	Beam width
Z	Reflectivity
K	refraction index
c	Light speed
r	Distance of the transmitter from the target

2.1.3 Main error sources on radar measurements

Radar performaces are affected by a certain numer of factors (fig: 2.2), a list of the more important include:

- ground clutter
- anomalous propagation
- partial and total beam blocking
- bright band
- attenuation

- beam broadening incomplete beam filling

Ground clutter is an unavoidable form of radar contamination. It occurs when fixed objects, such as buildings, trees, or terrain, obstruct the radar beam and produce non-meteorological echoes. Echoes resulting from ground clutter are usually exaggerated in both size and intensity and may cause radar systems to overestimate precipitation intensity in the area surrounding the radar. Clutter is usually found close to the antenna where the radar beam is nearest to the ground. Further out, the beam points gently skyward and overshoots most obstacles. Under certain circumstances, however, clutter may exist far away. A tall mountain range would be a good example of this. Clutter removal algorithms are developed for reducing this problem but often the key to dealing with ground clutter is still operator awareness and experience.

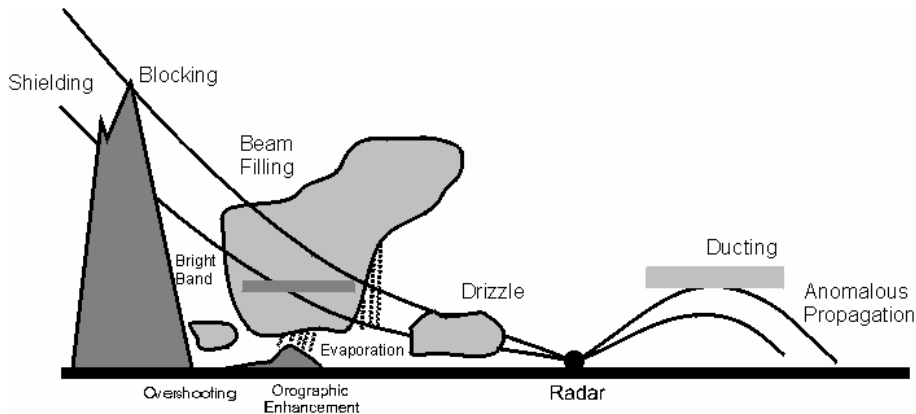


Figure 2.2: Schematic representation of the main problem related with radar performances

Anomalous propagation includes different forms of electromagnetic wave propagation that are not encountered in a standard atmosphere. Usually are observed when calm, stable atmospheric conditions, often associated with super refraction in a temperature inversion, direct the radar beam toward the ground.

Beam blocking, either partial or total, is obviously related with some huge obstacle, namely a mountain. It produces a cone of bad visibility where radar products are very bad.

Another effect related with radar measurements is the bright band, fig: 2.3. It may be seen in radar images as a narrow horizontal layer of stronger radar reflectivity in precipitations at that level in the atmosphere where

snow melts to form rain. As ice crystals fall toward warmer temperatures at lower heights, they tend to aggregate and form larger snowflakes. This growth accounts for an increase in radar reflectivity as the falling particles approach their melting point. As they cross the 0°C level, the particles begin melting from the surface inward and finally collapse into raindrops. The reflectivity maximum in the melting layer is partly accounted for by the difference in the value of the dielectric factor for water and ice. When a water film begins to form on a melting snowflake, its radar reflectivity may increase by as much as 6.5 dB because of the thermodynamic phase change. The reflectivity decreases below the melting level because when flakes collapse into raindrops, their fall velocities increase, causing a decrease in the number of precipitation particles per unit volume. The size of the particles also becomes smaller in the melting process, as their density increases from that of the snow and melting snow to that of liquid water. Both the reduction in size of the precipitation particles and the decrease in their concentration lead to a decrease in the strength of the radar echo at altitudes below the melting level, so that an isolated, horizontal layer of high reflectivity is established, usually centered about 100 m below the 0°C isotherm. The bright band is observed primarily in stratiform precipitation. The strong convective currents in active showers and thunderstorms tend to destroy the horizontal stratification which is essential for creating and sustaining the bright band.

Attenuation is the weakening of a radar beam as it moves downstream due to some of the energy being lost to scattering and absorption. The further a radar beam moves downstream the more dust, hydrometeors, etc. the radar beam will have to pass through. Because of attenuation, storms close to the radar are better sampled than storms far from the radar site. Beam spreading and attenuation both combine to produce a much poorer sampling of storms far from the radar. Attenuation is higher when the radar beam has to flow through a large number of hydrometeors. Storms and precipitation close to the radar degrade its energy before reaching storms further from the radar. Smaller wavelength radar beams attenuate more rapidly than long wavelength radar. Because of this, X-band radars have a shorter range of high clarity compared to the C-band one.

As pulses travel away from the antenna, the beam takes on a cone-like appearance and expands in all directions. This expansion or beam broadening increases pulse volume, resulting in decreased signal strength. Distant targets appear distorted, in fact, they may not be seen at all. Beam broadening also causes "partial beam filling," which implies that distant targets occupy proportionally less of an expanded beam. Thus, the true characteristics of a target may be hidden or altered during display. Beam broadening reduces azimuthal resolution and produces a form of radar nearsightedness. As the

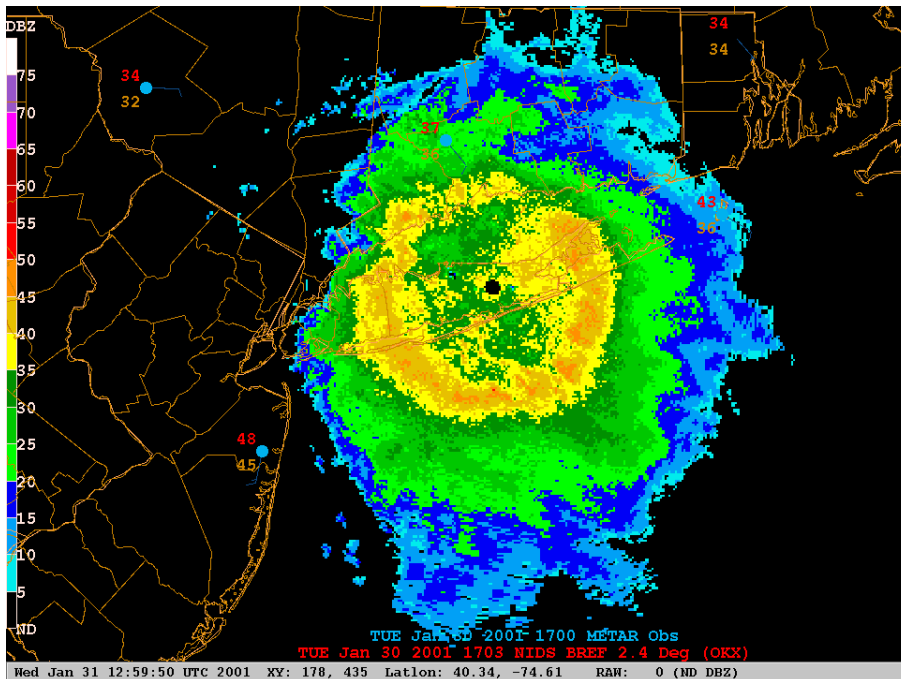


Figure 2.3: Clear example of bright band

beam diameter increases with distance, much more targets may occupy the beam simultaneously so that it may be difficult to see them correctly.

2.1.4 Principal radar displays

The plan position indicator (PPI), is the most common type of radar display. The radar antenna sends pulses while rotating 360 degrees around the radar site at a fixed angle. It can then change or repeat the angle according to the need. Return echoes from targets are received by the antenna and processed by the receiver.

It is to be noted that the height of the echoes increases with the distance to the radar, this change is not a straight line but a curve as the surface of the Earth is curved and sinks below the radar horizon.

An other important radar products is the range height indicator. A RHI is a radar display produced with fixed antenna azimuth and angle variable. In this way is possible to have a look of the vertical structure of the storm.

The last common radar display is the Constant Altitude Plan Position Indicator, better known as CAPPI. Is a radar display which gives a horizontal cross-section of data at constant altitude and is produced through analogic techniques that combines a spiral scan of the atmosphere.

2.2 The Veneto Radar network



Figure 2.4: Images of Mt. Grande radar

The Veneto Radar Network (VRN) consists of two EEC single polarization C-band Doppler radars, the former located on Mt. Grande (near Teolo) a 470 m hill top 25 km southwest of the city of Padova, the latter at sea level close to the border between Veneto and Friuli in northeast Italy (near Loncon). In fig: 2.5 positions of VRN. Their data are post processed by the Hydrometeorological Decision Support System (Conway et al. [2007]). This system integrates data from radars, rain gauges, satellite and numerical models to provide high resolution QPE and QPF.

The key components of HDSS include:

- radar quality control including clutter removal, bright band identification, hybrid scans and scan filling.
- mosaicking of Veneto radar
- data processing through a suite of applications named Quantitative Precipitation Estimation and Segregation Using Multiple Sensors (QPE-SUMS) (Gourley et al. [2001])

Data and product outputs are available via customized web pages and a three-dimensional graphical workstation, QPE is available every 15 minutes.

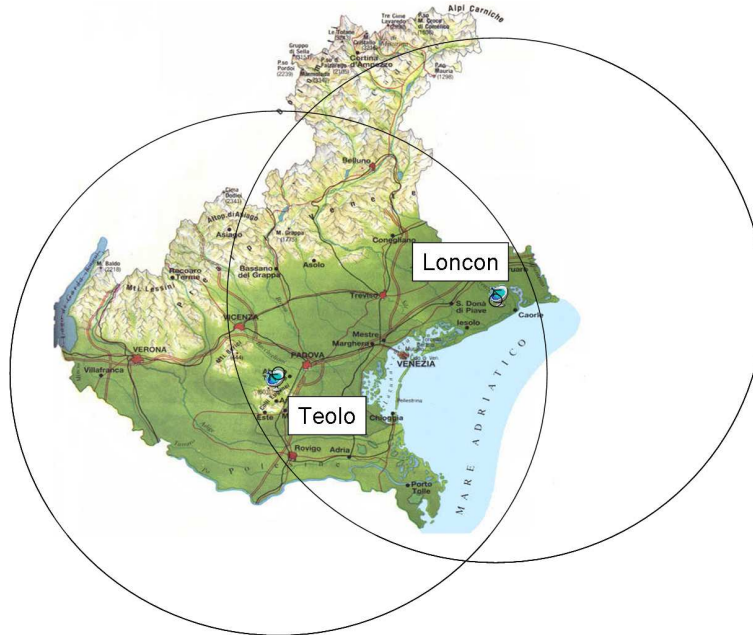


Figure 2.5: The veneto radar network(VRN)

2.3 The Swiss Radar network

The Swiss Radar Network ([Joss, 1998, SRN]) consists of three C-band Doppler radars providing full volume information every five minutes. The data are preprocessed and available on a Cartesian grid with a mesh size of $2 \times 2 \times 2 \text{ km}^2$ for the network composite.

The C-band radars Albis, La Dole and Lema are located on mountain tops at 925m, 1675m and 1625 m ASL, respectively. Fig: 2.6 shows Swiss radars locations.

MeteoSwiss has more than forty years of experience with radar operation in mountainous region. Many efforts went into the optimization of hardware stability and data processing for the radar network.

Several studies regarded variations in the reflectivity-rainfall (Z-R) relationship and beam attenuation (Germann and Gabella [2004]).

At, MeteoSwiss, large efforts has been spent into producing RAIN, a two-dimensional map with the best surface QPE over Switzerland. This product has achieved from his birth a great improvement on quality, Germann and Joss [2004a] for a better point of view.

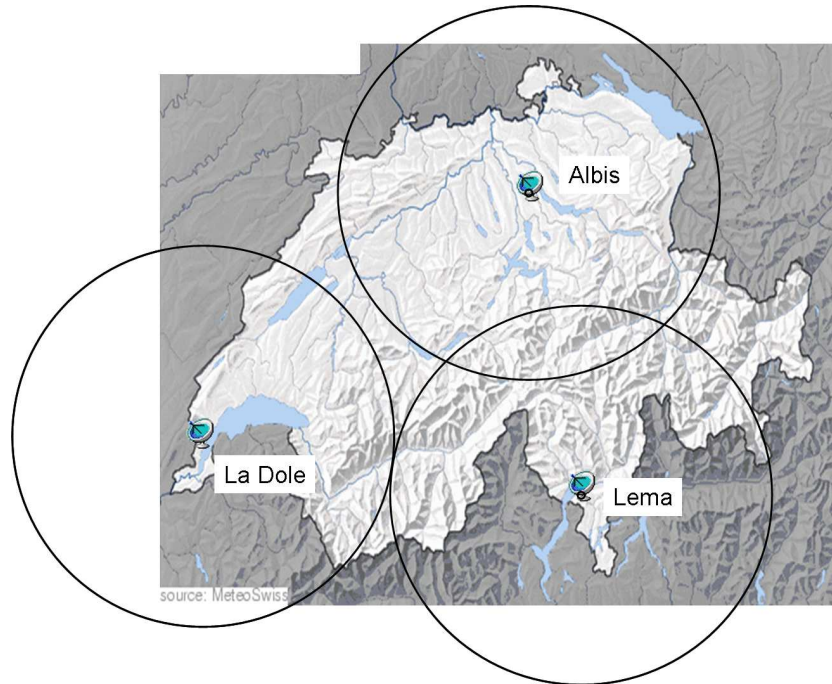


Figure 2.6: The swiss radar network(SRN)

2.4 The numerical model

The numerical model COSMO-2 is the operational MeteoSwiss implementation of the high-resolution version of the non-hydrostatic weather forecasting model of the COSMO (Consortium for small-scale modelling) community presently operational at several European Weather Services [Doms and Schättler, 2002, Steppeler et al., 2003]. The COSMO-2 model domain covers the Alpine arch (520 x 350 grid points, 60 vertical levels) and uses a horizontal mesh size of 2.2 km. The NWP system of MeteoSwiss, with the corresponding forecast domain at 7 km and 2.2 km is shown in fig: 2.7.

In the COSMO model the three-dimensional fully elastic and non-hydrostatic atmospheric equations are solved numerically with second or third order finite difference methods on a Arakawa- C/Lorenz grid based on a rotated geographical (lat/lon) coordinate system. No scale approximations are performed. Vertically a stretched terrain-following grid (Gal-Ghen and Somerville [1975]) is used and an option for the SLEVE vertical grid is also available

Prognostic variables include pressure perturbation, three wind components, temperature, specific humidity and turbulent kinetic energy. In addition, precipitation processes are explicitly described using a bulk-type cloud

microphysics scheme containing five prognostic hydrometeor types (rain, snow, cloud water, cloud ice and graupel).

The physics package of COSMO considers 6 main components: radiation, precipitation microphysics, convection, soil and surface processes, turbulence in the atmosphere and turbulent transport at the surface.

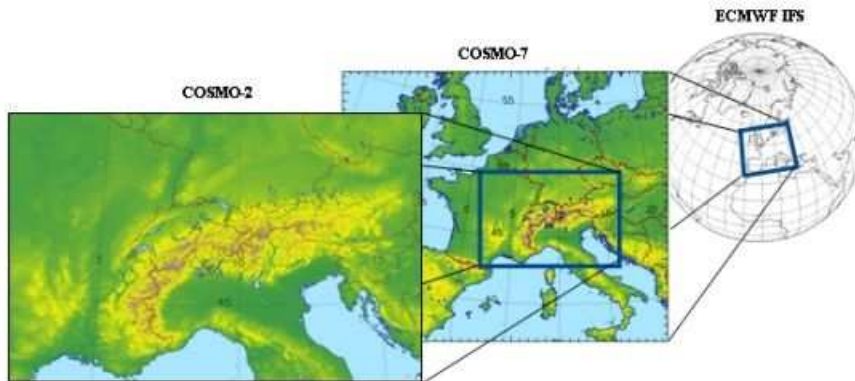


Figure 2.7: Setup of the MeteoSwiss NWP system based on the global model IFS for boundary conditions and initialisation of COSMO-7, COSMO-7 with 7 km horizontal resolution and COSMO-2 with 2.2 km resolution.

While shallow convection is parametrized, a parameterization for deep convection is not used. The COSMO-2 forecasts, covering the central Europe, are driven by the regional COSMO-7 model with 6.6km mesh size, which in turn is nested in the global IFS model of ECMWF. The COSMO-2 model uses a data assimilation system based on a nudging technique (Schraff [1997]) for conventional observations from surface stations, radiosondes, aircrafts and wind profiler. Assimilation of radar data with Latent Heat Nudging technique is possible for high resolution simulations (e.g. 2.2. Km), revisited by Leuenberger and Rossa [2007].

2.5 Data assimilation: LHN

Latent heat nudging (LHN) is a method which consists of forcing an NWP model towards observed precipitation rates. It is based on the observation that since relatively little moisture is stored in clouds, the column integrated latent heating rate must be approximately proportional to the precipitation rate. The principle is to correct the model's latent heating at each timestep by an amount calculated from the difference between observed and model estimated precipitation.

This extra heating then acts as a source term in the thermodynamic equation, which in turn brings about an adjustment in the model vertical velocity field that brings the model precipitation rate closer to that observed.

LHN used in this assimilations closely follow Jones and Macpherson [1997], contributions to LHN are related to the parametrisation of precipitation used. The LHN scheme thus used allows the prognostic treatment of precipitation as a variable and is advected in all three space dimensions. Stephan et al. [2008] proposed a modified LHN scheme to take into account the spatial and temporal separation of the rate of change in latent heating and surface precipitation and make the LHN algorithm better compatible with the prognostic precipitation scheme of the COSMO model. This improved LHN scheme is employed in operations in COSMO-2 and used in this study.

Single terms of LH equation are explained in table 2.2:

$$LH = \frac{\Delta T_{LH}^{mod}}{\Delta t} = \frac{L_V}{c_{pd}}(S_c - S_{ev}) + \frac{L_S}{c_{pd}}(S_{dep} + \frac{L_F}{c_{pd}}(S_{nuc} + S_{rim} + S_{frz} - S_{melt}))$$

Symbol	Definition / Description
L_V	Latent heat of vapourisation
L_V	Latent heat of sublimation
L_F	Latent heat of fusion
c_{pd}	Specific heat of dry air at constant pressure
S_c	Condensation and evaporation of cloud water
S_{ev}	Evaporation of rain in sub-cloud layer
S_{dep}	Depositional growth of snow
S_{nuc}	Initial formation of snow due to nucleation from cloud water
S_{rim}	Accretion of cloud water by snow (riming)
S_{frz}	Heterogeneous freezing of rain from snow
S_{melt}	Melting of snow due to form rain

Table 2.2: Terms in the LH equation

Forcing is distributed vertically consistency with model's parametrisation schemes and the temporal evolution of the profiles.

The scheme act on 3 steps:

1. Model physics and dynamic tendencies are derived from the current state of the model atmosphere.
2. The diabatic temperature tendencies related to phase changes of water for each grid point are calculated.

3. The LHN temperature increments for each grid points are calculated by scaling the profile by a factor related to the quality function if available (otherwise the scaling factor is equal to 1) and added to the prognostic temperature field at the end of the time step.

Then a LHN temperature increments ΔT_{LHN} is added to the prognostic temperature field.

$$\Delta T_{LHN} = (f - 1) \cdot \Delta T_{LHN_{mod}}$$

It depends on a scaling factor $f = \frac{RR_{ana}}{RR_{mod}}$ produced by the ratio of analysed and model rain rate, while $\Delta T_{LHN_{mod}}$ take into account the model LH tendencies.

In order to analyse rain rates, we consider a weighted sum of the radar-estimated and the model rain rate:

$$RR_{ana} = w(x, y) \cdot RR_{rad} - [(1 - w(x, y))] \cdot RR_{mod}$$

For $w(x, y) = 1$ radarm measurement are considered extremely dependable, so that the analysed rain rate is equal to the radar-estimated rain rate, while for $w(x, y) = 0$ the observations are rejected and the analysed rain rate is assumed to be equal to the model rain rate.

2.6 Data set

Radar products, different for Veneto and Switzerland, has been treated through IDL (Interactive Data Language), a very powerful programming language for analyzing and visualizing data. New routines has been created for Data analysis and to prepare grib files for radar data assimilation.

Table: 2.3 provides an overlook on the main features of these data sets:

Table 2.3: Features of data sets

Case	Period	Time step	File type
Veneto	From 2005	Every 15 minutes	NetCDF
Swiss	From 2005	Every 5 minutes	Gif

Each Veneto file contain various variables, like rain or snow precipitation estimate for 1 and 3 hours and instantaneous rain rate, with relative scale factor to apply to them. Informations pertaining to the radar domain are

also present in these NetCDF files. Swiss files used are very slim compared to Veneto and contain only instantaneous estimated rain.

Chapter 3

Derivation of an empirical radar data quality description

During last few years interest in radar data quality is risen a lot. This is due principally to two fact: the increasing of quantitative use of radar observations in hydrology and the assimilation of these data in statistical framework as variational assimilation, this bring to unsolved problems.

For operational uses we need a description of data quality in order to avoid assimilation of gross errors or zero values where the radar is not able to work properly.

A pragmatic approach like the radar data quality function produced during this thesis work, instead of investigating the error covariance matrix (like Keeler and Ellis [2000], Berenguer and Zawadzki [2008]), can be an alternative way to approach the problem.

Germann and Joss [2004b] show that a long-term precipitation accumulation reflects the radar visibility. From this starting point the empirical approach for producing this radar data quality function is that also frequencies of occurrence can reflect radar visibility under right condition like long term accumulation and range attenuation.

3.1 Analysis on frequencies of occurrence

This kind of analysis has been chosen because of a direct relationship between frequencies of occurrence, visibility and range.

It is based on the assumption that everywhere, on long term accumulation, the same frequency is steady and differences are only quantitative. So frequencies became lower and lower when we move from good to sub-optimal visibility areas, while totally shielded zones have frequencies near zero.

At the same time, pixels that belong to high percentiles of f are most likely non rain echoes.

In fig: 3.1 is possible to compare rain accumulation and frequencies of occurrence for Veneto and Swiss radar networks and it is self evident that the same features are reported.

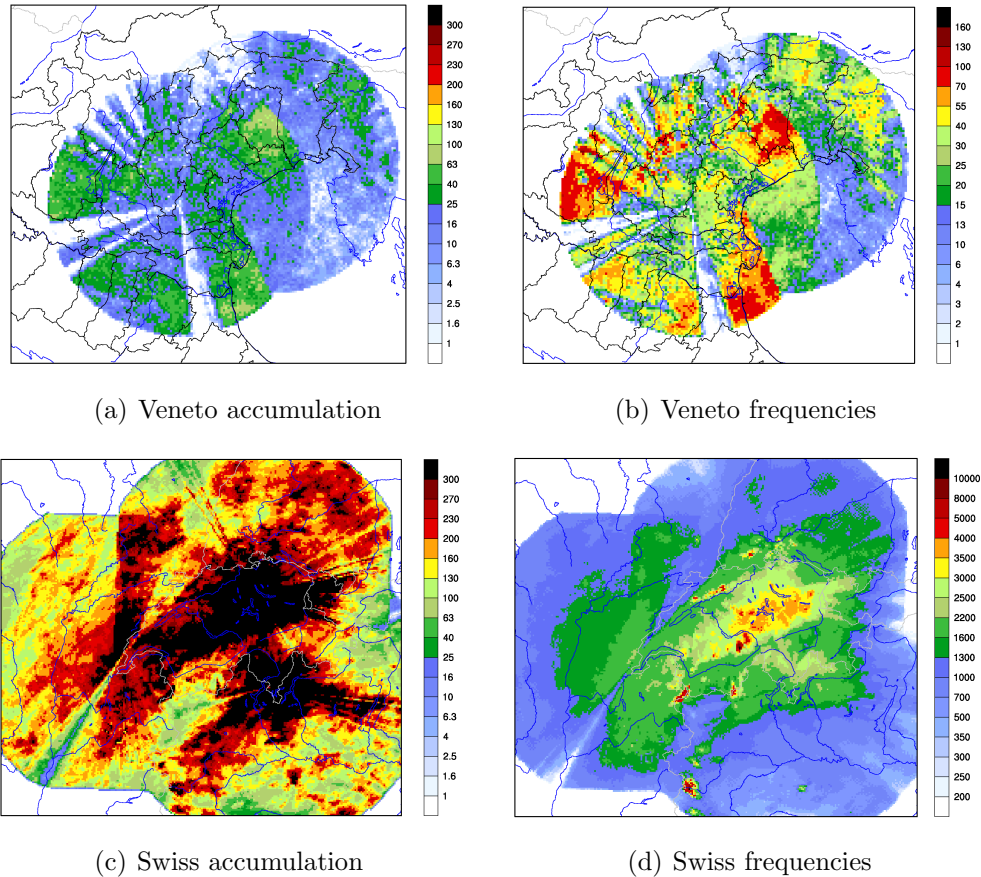


Figure 3.1: Accumulation and frequencies for VRN and SRN for a Summer (JJA) period. Pay attention to different frequency label between Veneto and Swiss.

Other than similarity between accumulation and frequency, in this images are clearly shown the principal features related to quality of radar data like sub-optimal visibility and clutter. In fact, shielding from obstacles nearby the radar sites produces cone with null or low visibility.

The most relevant among these are, for Veneto radars, the one produced on South-East direction which is produced by Mount Venda and two more on W-S-W direction which are in turn produced by Mount Madonna. In the

upper part of Veneto images is also visible the shading produced by the alps on the radar beam.

For Swiss radar network the main cones are related with La Dole instrument and are in S-W and N-E direction.

Areas with lower visibility are related also to deep valleys and with range effects. All swiss radars are placed up from 900 m asl and this can bring to have lower visibility areas in presence of deep valleys. On images are visible two zones with lower f that is possible to identify with Grisons and Valais. These two deep valleys are sensibly lower than radar sites and happens that some precipitation may be looses. Range effects are also clearly visible with frequencies and accumulation that constantly decrease going away from radars.

Finally, clutter is present in all images and is recognizable in isolated pixels with very high frequencies and accumulations.

For a better point of view of informations on informations related with long-term frequency of QPE occurrence we applied a kind of normalization producing the percentage of frequencies of occurrence, that only permits better comparing and keep quality of information unchanged.

In this kind of plots are still clearly visible range attenuation, cone, deep valley and clutter.

These analyses have been fraught with some problems, though different between Veneto and Swiss data-sets.

Nearby the radars Veneto data have, in fact, yielded frequencies lower than those far from the radar without any range effect.. This is probably due to calibration problems ,since in the last accumulations of 2009, this problem seems to be less evident.

Swiss radar data used, instead, were raw with a less efficient clutter removal.

Application of a speckle filter has been necessary for cleaning data. Speckle filter in homogeneous areas preserve information and edges but remove a good number of clutter pixels as we can see on fig: 3.2. On the bottom part of figures is clearly visible the effectiveness of removing clutter of this filter.

3.2 Rest clutter identification

The main problem with rest clutter pixels is related with their identification, our approach in this work has been pointed to analysis of auto-correlation of single pixel time series.

If we produce time series of pixels over a period long enough, probable clutter pixels have demonstrated to have non zero signal in an absolutely ran-

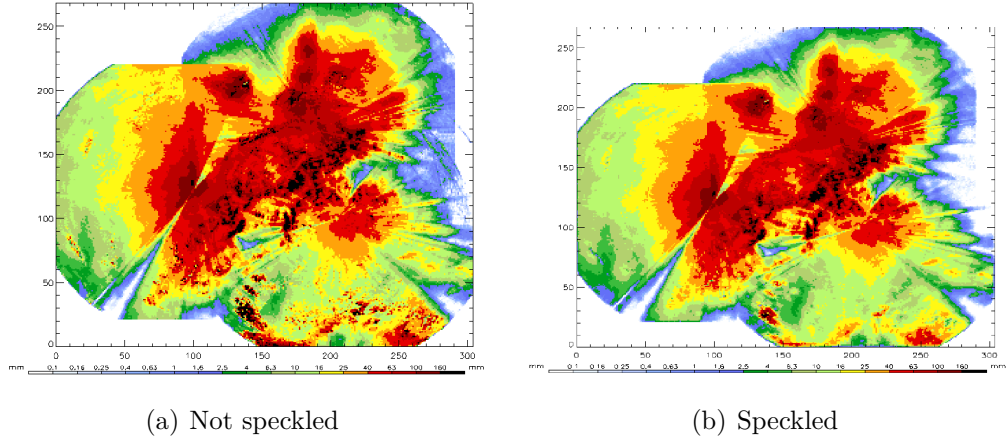


Figure 3.2: Accumulation with and without speckle filter for 2007 Summer period.

dom way. Rainy pixels, instead, have same periods with no signal alternate with consecutive time steps with signal detected.

We can see this in fig: 3.3 , where are visible 4 time-series, autocorrelations and derivatives of them. We have 3 pixel with similar signal (nr. 1,2,4) which can be identified as rain while, the third, that has a different behaviour with something like noise superimposed to rain.

Auto-correlation functions used by IDL processes have this formulation:

$$P_L(x) = \frac{\sum_{k=0}^{N-L-1} (x_k - \bar{x})(x_{k+L} - \bar{x})}{\sum_{k=0}^{N-1} (x_k - \bar{x})^2}$$

Pixels with random behaviour have an auto-correlation that decreases in a steeper way than rain pixel as we can see on bottom left panel.

Some problem with clutter identification has became from Veneto data due to lower frequencies of occurrence related to lower frequency of radar sampling, every 15 minutes insted 5 of Swiss radar network. This bring, for an equal period of accumulation, to slighter differences between rain and clutter pixel (loose of auto-correlation in 15 minutes is more sensible than in 5) with obvious problems on clutter identification.

This problem is supplied by the clutter removal algorithm applied to the Veneto radar data that have demonstrated to be very efficient.

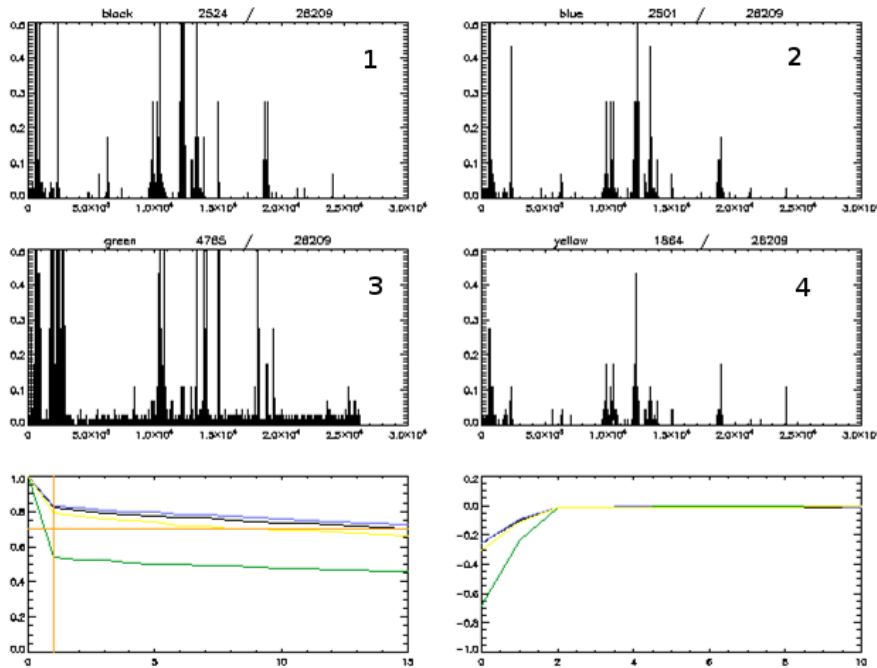


Figure 3.3: Time series for 4 pixels, one probably clutter (nr. 3), auto-correlations of them and derivative of auto-correlations.

3.3 Quality function construction

The construction of an empirical radar data quality function here shown is based on long-term frequency of QPE occurrence analysis and take into account:

- sub-optimal visibility areas
- clutter pixels
- range effects

Sub-optimal visibility areas are identified by low frequencies of occurrence, clutter pixels through auto-correlation and we provide to account for range attenuation through a $g(f)$ function, applied from an f_0 threshold.

The procedure enacted to generate the daily radar data quality function is based on the analysis of a previous long period, and can be summarized in 3 steps:

1. loading the previous period pixels information of:

- percentage of frequencies of occurrence
 - time series of 0.92 percentiles in frequency (in this group of pixel we search for rest clutter ones).
2. updating all pixel informations by adding the next day and subtracting the first day of the series
 3. Building of weighting function like this:

$$w(x, y) = \begin{cases} 0 & \text{For rest clutter pixels} \\ g(f) & \text{For pixel under the value of } f_0 \\ 1 & \text{Elsewhere} \end{cases}$$

Identification of rest clutter pixel is carried out by evaluation of a limit, $a'(0)_{min}$, on derivative of auto-correlation at $t = 0$. If $a'(0) = (\frac{da(t)}{dt})_{t=0} \leq a'(0)_{min}$ we identify this pixel as clutter.

The $a'(0)_{min}$ limit has been chosen in empirical way through time series analysis of a great number of cases and has been set to -0.4 .

Function $g(f)$ should take care of range effects on radar beam, such as beam rising and its broadening as well, with special care to transition between good pixel, with $w(x, y) = 1$, to pixel with quality slightly worse. For this reason a function like:

$$g(f) = 1 - \frac{1}{1 + e^{(\frac{10-f}{7})-4}}$$

which decrease slowly from 1 at the beginning, while, after, its value goes down faster. In fig: 3.4 the weighting function concept related with frequencies of occurrence is resumed.

The choice of f_0 and of the period of accumulation for the information to update are pivotal for quality function construction.

The f_0 value can be seen as the border between good pixels and those ones affected by range effects; it has been evaluated in empirical way through many tests compared with the literature on range quality of radar data.

In table: 3.3 it is possible to see values of f_0 for quality functions, to remark a great difference probably due to different calibrations of the two radar networks.

Another choice to be made for the construction of the weighting function regards the length of the accumulation period used as pixel information on step 1. In the perspective of updating such an analysis by adding the latest day while taking out the oldest in the data set, the length of the period should be long enough to avoid too large day-by-day variability, while it should be short enough to allow for at least seasonal differences.

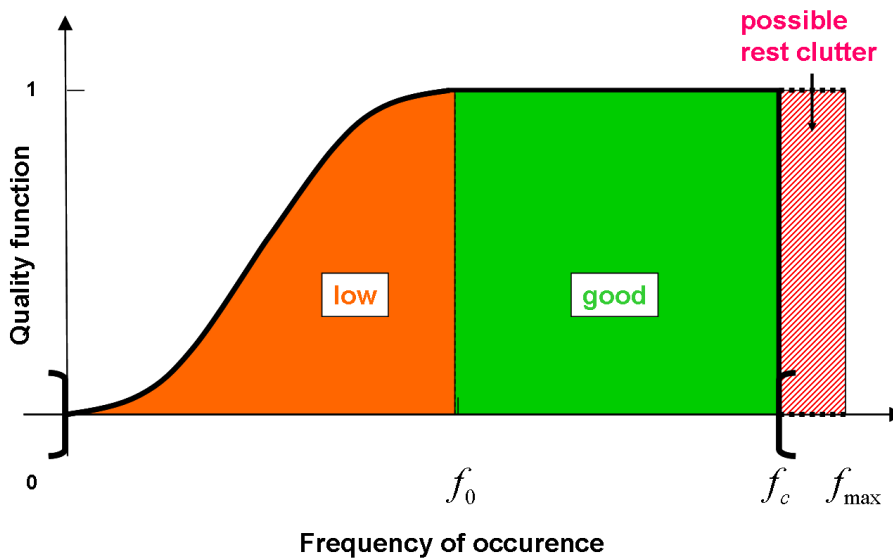


Figure 3.4: Conceptual definition of the radar data quality function.

One-month periods proved to be rather short, while three-month periods seem more adequate. In fact, provided a thirty days period, 1 days is approximately 3%. If we add a no rainy day and subtract a day with a lot of signal we can arrive to loose near the 6% of signal.

This produces a very unstable quality function. Three months accumulations seems to be a good choice

Table 3.1: Values of f_0 for Veneto and Swiss radar networks

Radar Network	f_0 value
Veneto	0.4%
Swiss	7%

3.4 Results

Final results for Veneto radar data quality function can be seen in figure 3.5. Mount Venda and Mount Madonna cones (the two closeby hill peaks) are clearly outlined in $w(x, y)$, as are the shielded areas behind the prealpine chain to the north.

The range effects, however, is inverted, showing good quality at longer and reduced quality at shorter ranges; this issue can still be probably included

in calibration problems of VRN, but still needs a clear explanation. Also, there is a significant difference between the two radars in the network.

The seasonal variability is also plausible in that in summer the precipitation systems are higher-reaching than in winter so that they are seen at longer ranges in summer yielding better quality. Particularly Alpin areas are present in Summer quality function due to high convective phenomena.

Figure 3.5 shows the results for summer and winter seasons in the Swiss radar network. It can be easily seen that the main and well known error prone areas are reproduced by the quality function, i.e. the scarce visibility in the valleys like the Valais and the Engadin, the cones due to nearby obstacles of the La Dole radar, the range effect in all three radars, as well as a number of small scale clutter-prone areas.

The seasonal differences are well in line with those found for the VRN. The most evident features include the longer ranges over the mountains to the north. In particular, the quality at long ranges is reduced in winter, when the orographic blocking as well as the cone of the La Dole radar extending to the northeast are much more pronounced. The rest clutter pixels (white wholes) are remarkably stable and tend to be larger in winter than in summer. Swiss radar data, as explained above, most likely have a better calibration and this produces a better quality function. We can see cone areas, especially those from La Dole, and Grison and Valais deep valleys.

Range attenuation effects are evident, similar for La Dolee and Albis, fewer for Lema. This behaviour of Lema radar is yet to be explained.

May is due to a period of maintenance of this radar that has bring to a lower number of rain event reported.

There is also an evident seasonal variability, plausible in that in summer the precipitation systems are higher than in winter resulting in better visibility, thus yielding better quality at far ranges.

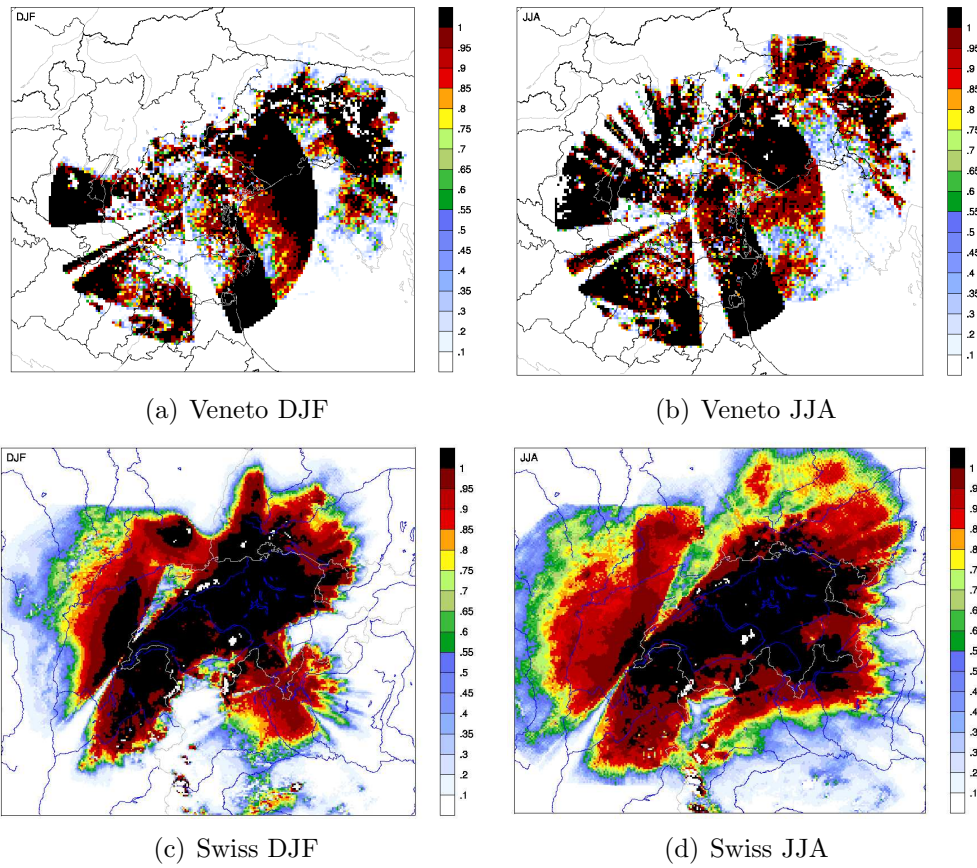


Figure 3.5: Radar data quality function for VRN and SRN for winter and summer period.

Chapter 4

Assimilation experiments

The choice of case studies is fundamental for the interpretation of the real quality of results and it should be calibrated for optimizing evaluations in the field under investigation. In this thesis work we have two radar networks and almost one case for each has been chosen: Veneto radar data assimilation had never been done before, so not only the impact of the quality function but also effect of LHN scheme have to be investigated.

In the Swiss case, allowing for previous experiments on radar data assimilation, the study was focused only on quality function to try to understand if it has some effects on problems related to latent heat nudging use like border effect due to bad quality of far radar data.

4.1 Experimental setup and diagnostic material

Experiments has been developed on cray XT-4, Buin, at the CSCS (Swiss national supercomputing center). The whole range of experiments carried out is shown in table: 4.1. They can be split into assimilations and forecasts and, only for assimilations, those on the use of LHN with or without the radar data quality function.

Some products of COSMO-2 experiments have been used to analyse impact of LHN and quality function on the cases.

The software used for plotting model products is NCL (NCAR Command Language). A free interpreted language designed at the National Center for Atmospheric Research specifically for meteorological data analysis and visualization.

The various maps developed have regarded:

- Total event cumulated rain maps
- 1-hour cumulated rain
- Low level winds
- Vertical section of equivalent potential temperature at various Latitude and Longitude
- Relative humidity at 850 hPa
- Divergence and vorticity at 9000 a.s.l.m.
- Vertical section of sums on all time steps of vertical velocity at various Latitude and Longitude
- Sums on all time steps of divergence and vorticity at 2000 a.s.l.m.

Table 4.1: Assimilation experiments for the assessment of the impact of the radar data quality function on the LHN scheme.

experiment	description	SRN case	Veneto case
REF	without LHN	48h from 11 Aug 2008 00UTC	24h from 26 Sep 2007 00UTC
REF_R	with LHN, without quality function		
REF_RQ	with LHN, with quality function		
FC03	forecast, with LHN, with quality function	not for Swiss case	21h from 26 Sep 2007 03UTC
FC06			18h from 26 Sep 2007 06UTC

Experiments REF_R and REF_RQ have also been replicated by forcing radar data on assimilation halved and doubled for investigate the sensitivity of the LHN scheme [Rossa and Leuenbeger, 2008]

4.2 Case descriptions

In this section a synoptic description with an analysis of chosen event is performed.

4.2.1 Mestre flood

This rainfall event was exceptional in terms of rainfall intensities and accumulations (up to 120 mm/h , $90\text{ mm}/30\text{ min}$, and $24\text{ mm}/5\text{ min}$), overall accumulation reached $320\text{ mm}/6\text{ h}$ and caused flooding of the urbanized area

of Venice Mestre. A surface low located on the Gulf of Genoa was associated with an upper-level trough which advected cold air from Northern Europe towards the Alps and subsequently onto Veneto, giving rise to organized convective activity.

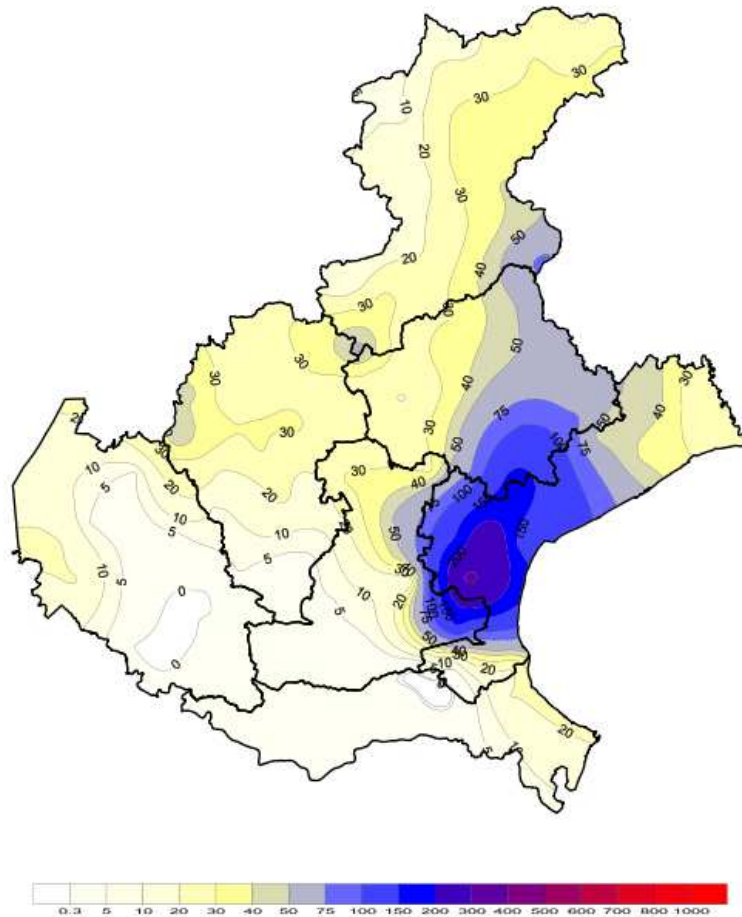


Figure 4.1: Veneto rain gauges accumulation of 26 september

From midnight to the early morning hours convective cells developed, among these, two of which showed clear supercell signatures. Towards 04 UTC the type of convection changed from supercellular to multicellular when low-level warm and humid Adriatic air began feeding directly into the system from the east to form a mesoscale convective system (MCS). The flow configuration at this stage was such that the continuous regeneration of convective cells took place in the relatively circumscribed area of $20 \times 40 \text{ km}^2$ around and west of Venice Mestre. The MCS became quasi-stationary for about 4 hours, during which the exceptionally high rainfall rates and accumulations were

recorded. After about 08 UTC the MCS propagated slowly eastwards and reached the Adriatic Sea by early afternoon. Accordingly, the rain started to decrease after 08 UTC and stopped over the area of interest after midday. The MCS still exhibited significant rain intensities throughout the afternoon, though located over the Sea.

A map, produced by ARPAV rain gauges network, of the daily rain accumulation is shown in fig: 4.1.

The COSMO-2 analysis cycle confirms the heavy precipitation, though with incorrect timing and extension. As a matter of fact, a first passage takes place between about four hours later between 08 and 12 UTC and hits a much larger area. Six hours later a second passage with similar spatial extension and even larger intensities flows over the region. Both passages seem to be associated with an upper-level disturbance, visible in the vorticity field (not shown). The observed precipitation maximum is not coincident with the one in the analysis cycle.

Bad description from the model of an heavy convection event like this is a very good motivation to test the LHN scheme for assimilation of radar data on Veneto domain.

4.2.2 Swiss cases

The case studied over the SRN domain is a less exceptional case of the passage of several frontal rain bands over Switzerland. We can have an overview of this fact with some rain gauge data in table 4.2.

Table 4.2: Precipitation measured by rain gauge for 11-12/08/08

Station	Precipitation (mm)
Neuchatel	72
La Dole	70
Basel	58
Geneve	52
Bern	47
Chur	14

On 11 August 2008 an extensive long wave trough was situated over Western Europe. An associated low pressure system over the British Isles with a core of 990 hPa was associated to a warm and a cold frontal passage in central Europe on that and the following day.

On 11 August in the afternoon, a first rainband associated with the warm front crossed Switzerland, causing up to 18 mm of precipitation. In

the night the coldfront entered the SRN domain from west and passed slowly over Switzerland during the 12 August. This coldfront led to heavy frontal and convective rainfall with sums up to 70 mm in northern Switzerland.

Chapter 5

Results

In the following sections results on assimilation of radar data and impact of quality function are analysed.

5.1 Mestre case

5.1.1 Results on assimilation of radar data

The impact of Laten Heat Nudging scheme is shown on fig: 5.1, panel a. It manages to moderate precipitation to a large extent, for instance reducing values of more than 100 mm in the the area northwest of Mestre to under 40 mm (20 mm) for the greenish (blueish) colors.

The highest accumulations simulated just to the east of Mestre were almost entirely suppressed in the LHN run. On the other hand, it successfully triggers the precipitation in the area where it was observed with about the right accumulation, as we can see comparing model results with rain gauges measurements (fig: 4.1).

Strikingly, the LHN REF_R run induces more precipitation at the border, visible, expecially at south-west, in a clear dipolar structure in the difference field. The highest accumulations simulated just to the east of Mestre were almost entirely suppressed in this run.

The assimilation scheme also forces the model to represent Mestre deep convection event. It successfully triggers the precipitation in the area where it was observed with about the right accumulation (fig: 4.1) and good timing. This is visible on accumulation maximum in Venice area and in the hourly accumualtion maps (not shown).

The LHN has a very large impact on the simulation in analysis mode featuring a very efficient drying of the excess precipitation and excellent

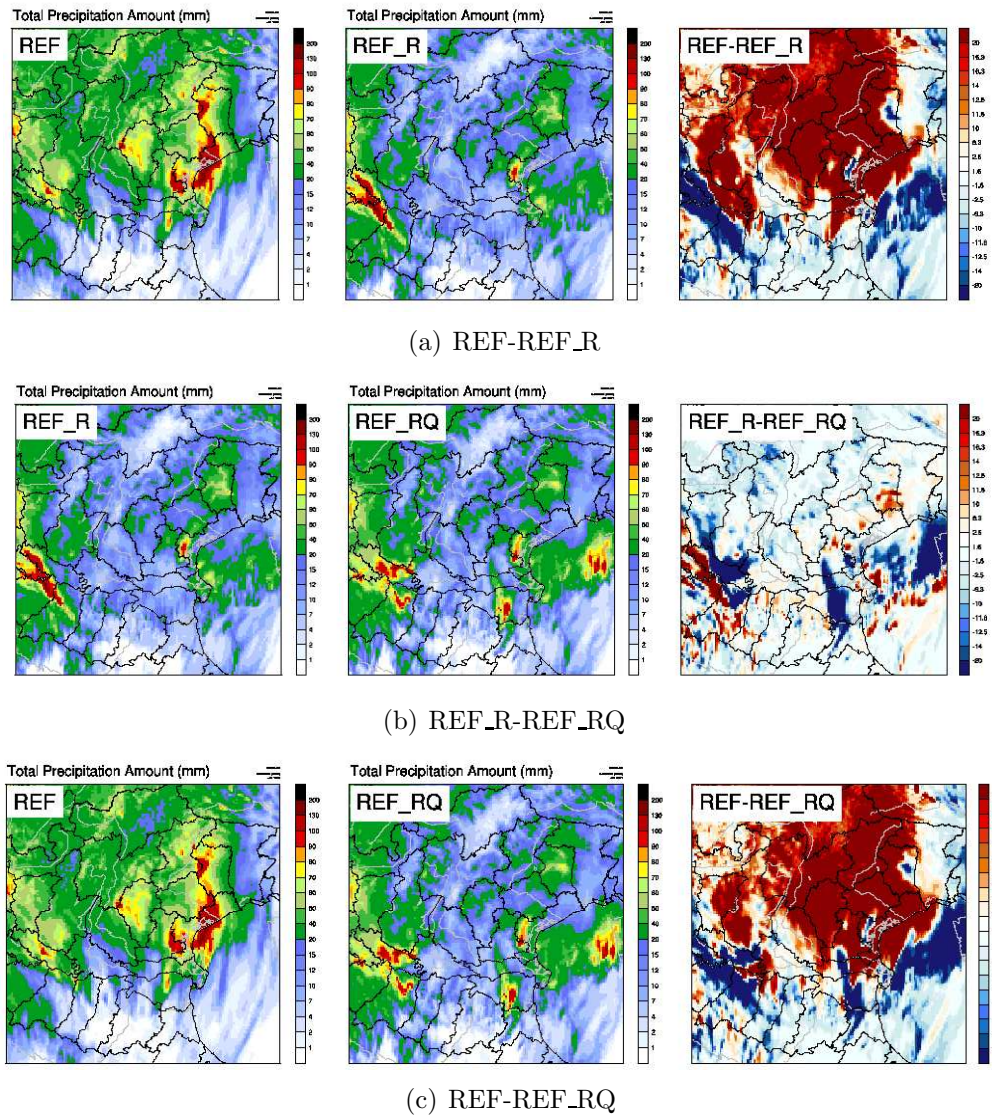


Figure 5.1: 24h accumulation of the Veneto case

triggering of the observed convection. There is a clear response of the low-level wind and convergence field illustrating that the LHN method is able to modify the microscale circulation around the precipitation system, this is shown with the low level wind map in fig: 5.2.

The positive impact of the LHN in analysis mode is carried over in the free forecast mode for about 2-3 hours, after which the 'wrong' upper-level dynamics takes over and reintroduces the incorrect precipitation systems. In

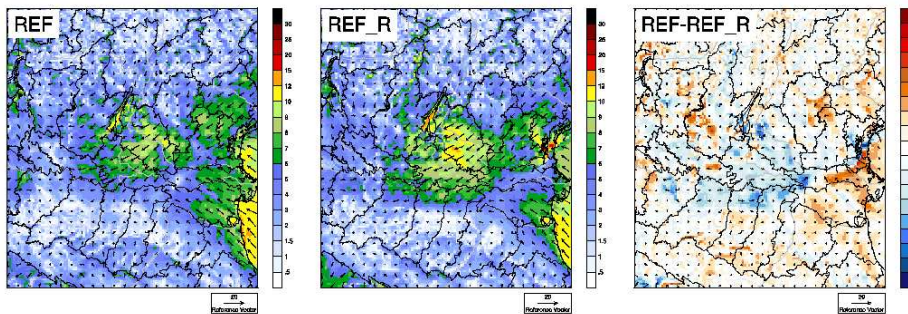


Figure 5.2: 06UTC wind direction and strength at the model lowest level for REF and REF_R experiments.

figure 5.3 it is possible to see that the deep convective system on Mestre area regresses from his right position with the next time steps. This pinpoints the limitation of the LHN to substantially modify the mesoscale circulation, especially upstream and at upper levels.

Not optimal behaviours of Latent Heat Nudging are typically connected with areas that are badly seen by radars. Since the LHN acts to adjust the model's latent heating profile such that it is compatible with the surface rain rate, this extra heating, or cooling, then acts as a source term in the prognostic model temperature equation and thus introduces changes in the buoyancy, which in turn affects the precipitation building processes.

Suppose that the model has precipitation in an area which are badly seen by the radar. Without accounting for this reduced radar quality the LHN scheme tries to reduce or suppress the model precipitation by cooling the profile, which can induce subsidence (Fig. 5.4). If this happens close to a boundary of the radar domain such a subsidence can act to produce an outflow boundary which, in turn, can create a low-level convergence able to trigger precipitation. Fig: 5.1, REF_R, indeed shows that the precipitation field exhibits an artificially looking structure close to the left border of the radar domain.

Fig: 5.5 shows, on a section through the artifact border structure, the sum of vertical velocity of each time step of the day. The border of radar domain is situated at 10°E , just at the center of the image. An area is present east of the border where cooling produces subsidence for all the day, this area is between 10°E and 10.4°E , higher than 2000 asl, and it coincides with a cone area. Just out the border of radar coverage divergence of this air mass forces air to lift and this create the rain band. Subsidence is produced till 2000 m asl because of a LHN setting that apply LHN scaling of model LH

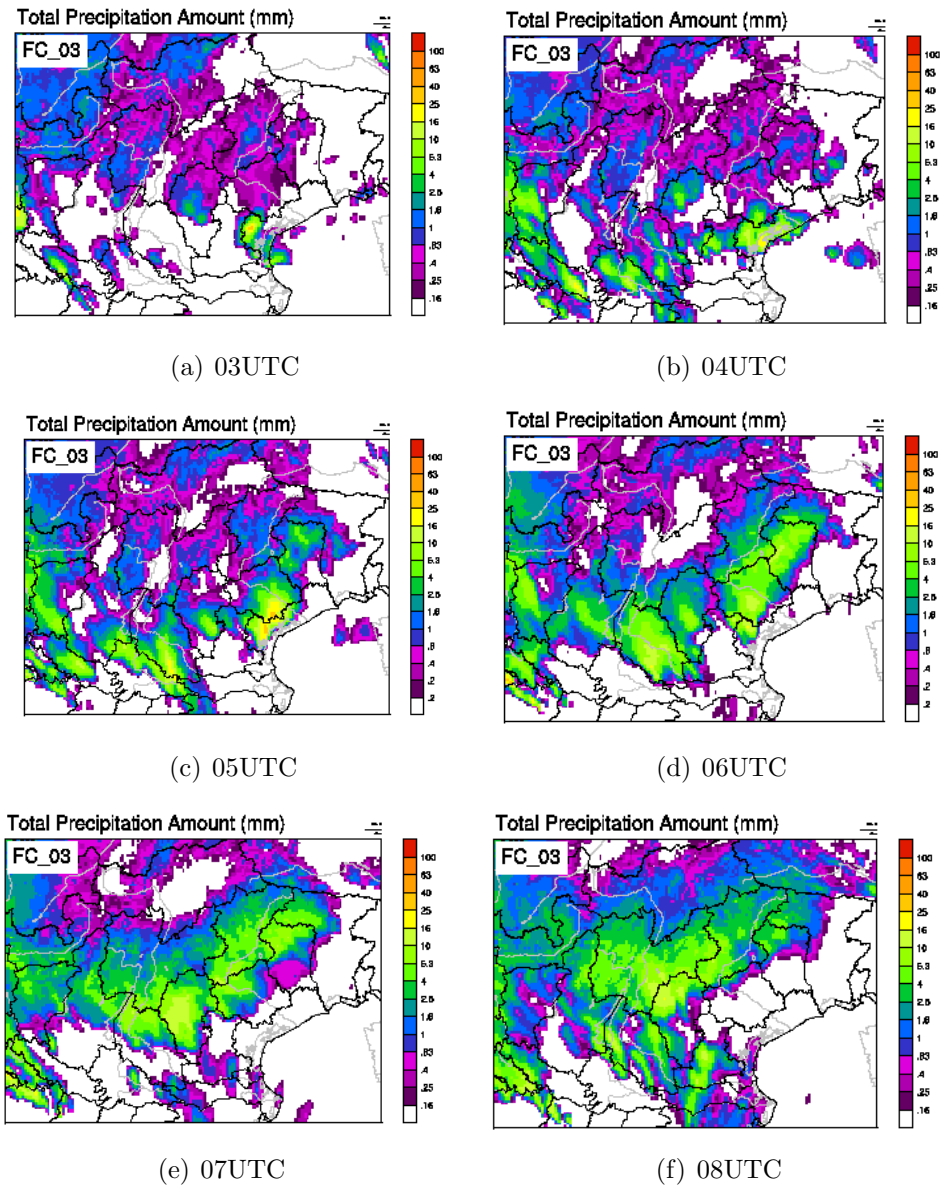


Figure 5.3: Hourly accumulation for a forecast experiment. Radar data are assimilated until 03UTC then the model is free to evolve.

only till cloud model base.

Sensitivity of the LHN scheme to radar forcing has been investigated through two experiments with radar data halved and doubled in their values (fig: 5.6).

In panels where differences are plotted different behaviours of the model

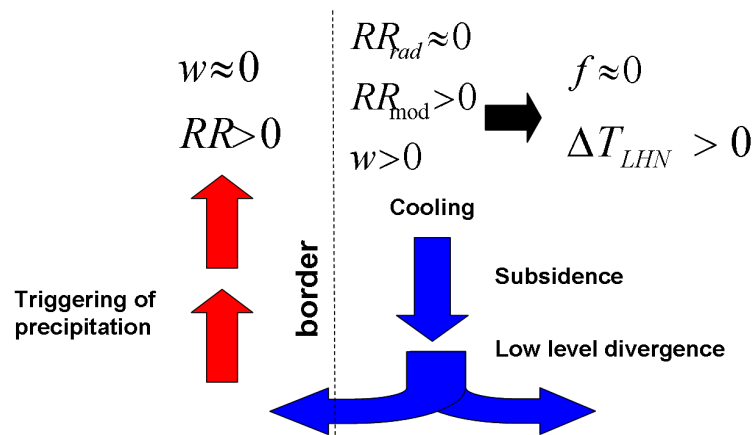


Figure 5.4: Conceptual sketch of what can happen at the border of a radar domain when no radar data quality is accounted for in the LHN scheme.

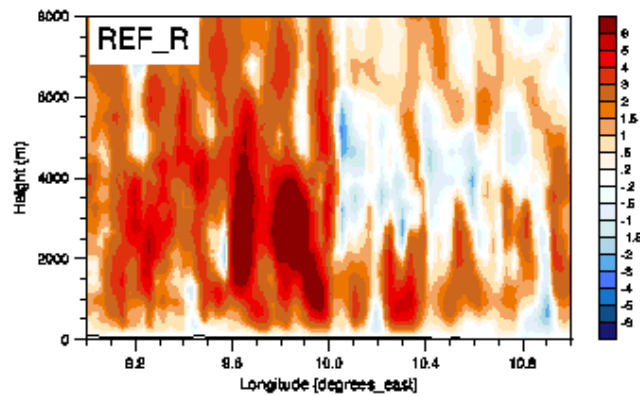


Figure 5.5: Section at 44°N of sums of vertical velocities. The border of radar domain is at 10°N.

to LHN are noticeable. Where assimilated radar data are other than zero, the model response is lighter (greater) than normal case according to halved (doubled) forcing. Rain amounts are perfectly compatible with Leuenberger and Rossa [2007], in fact, in the case of underestimation (overestimation), the cumulated rain is not halved (doubled), but amounts to 80% (120%) of the not scaled experiment.

In areas with no radar signal the drying effect of LHN is not affected by a greater (lighter) forcing and the same quantity of accumulation is still present.

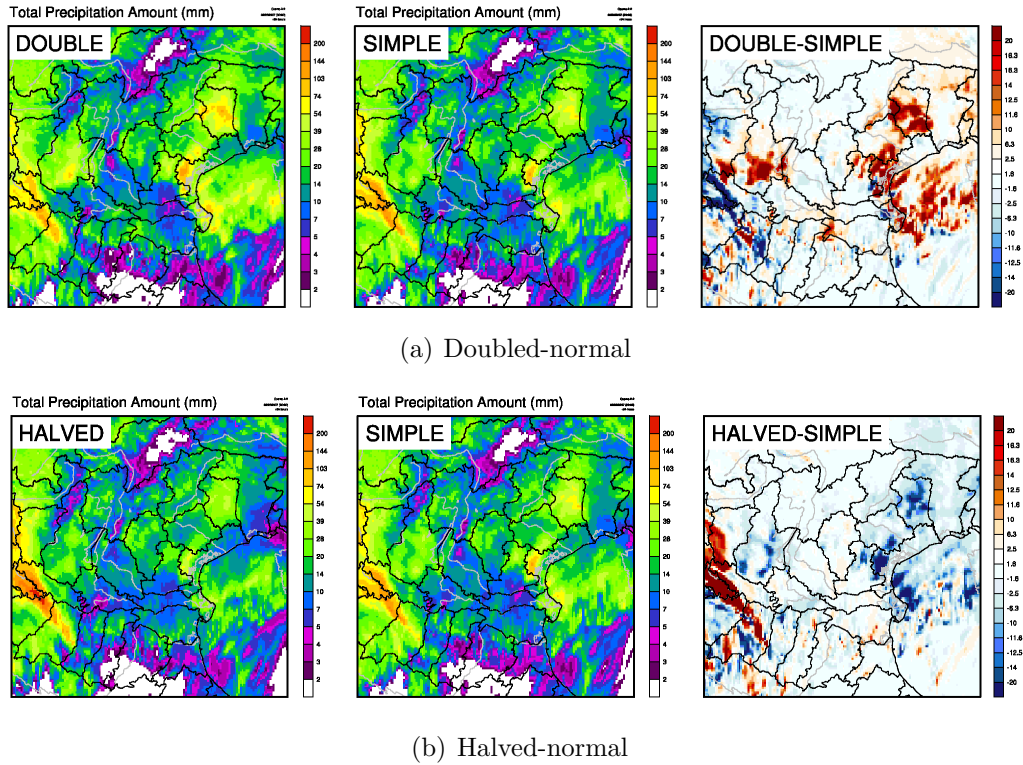


Figure 5.6: Differences between REF_R cases with radar data forcing normal, doubled and halved

At border areas there are also differences, with increasing of radar signal (RR_{rad}) the border artificial rain band decrease. This is due to RR_{mod} that is constant and always greater than RR_{rad} , so we have $1 \geq f_{double} \geq f_{normal} \geq f_{halved}$. As consequence we have always $\Delta T_{LHN} \leq 0$ (the forcing term added to temperature field), but lower and lower in the absolute values with increasing of radar assimilated signal. This bring to produce less cooling and less subsidence with a reduction of divergence and air forced to lift.

5.1.2 Quality function results

The main impact of the quality function in the experiment REF_RQ as compared to REF_R is the reduced dipolar structure at the western border (Fig: 5.1) of the radar domain and, most prominently, the differences in the blind cones of the Mt. Grande and Mt. Madonna.

The border precipitation band is markedly reduced in intensity. In fact, daily accumulation passes from values up to $130mm$ to values near $60-70mm$.

In the cone areas the quality function allows for the model precipitation to remain within the simulation. More subtly, and due to the fact that the quality function of the Veneto radar network is 1 around these areas, the cone constitutes a border between the areas where the radar is assigned 0 and full quality. In this case, the erroneous model rainfall is suppressed by inducing subsidence (Fig: 5.4), but not in the cone, so that the resulting low-level outflow produces a convergence and, therefore, enhanced rainfall with high daily value (till 100mm).

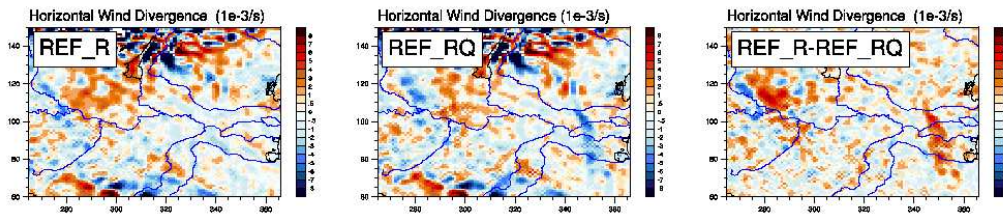


Figure 5.7: Divergence at 2000 aslm for REF_R and REF_RQ experiments.

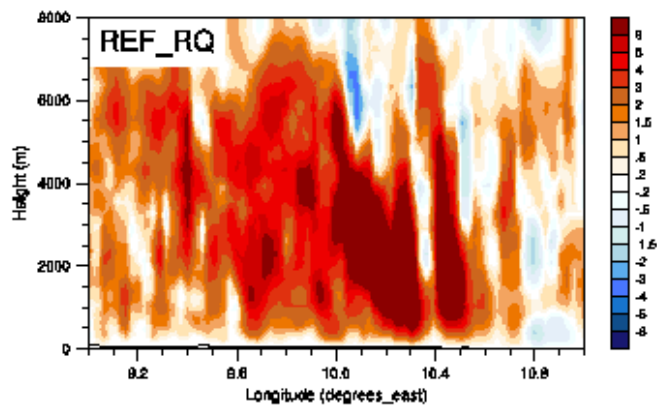


Figure 5.8: Section at 44°N of latitude of sums of vertical velocity

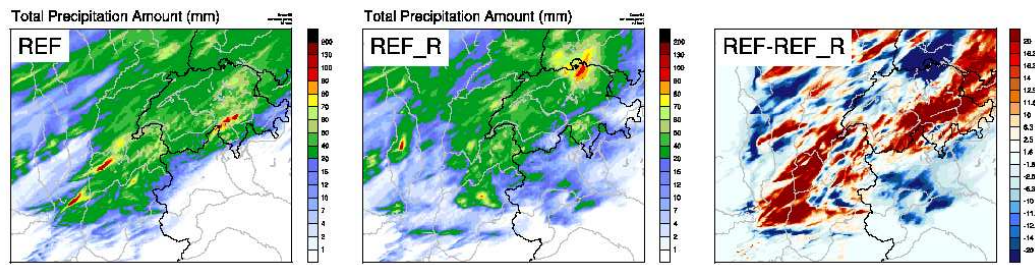
In fig: 5.7 we can appreciate from divergence at 2000 aslm how there are convergence areas in the cone zones in the REF_RQ experiment; this is particularly evident for Mt. Grande (the cone towards S-E). We have another sign of this behaviour in the sum of vertical velocity on a vertical section, through the cone and border area, for all the time steps (fig: 5.8).

We can observe an area, coincident with the cone, where we have positive vertical velocity rather than subsidence and this is associated with the artificial rain phenomenon in the LHN scheme with quality function (LHNQ). On

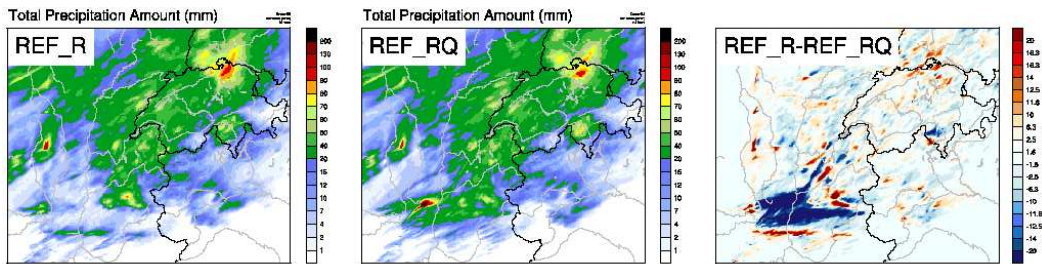
the border area (between 9.8°E and 10°E), instead, vertical velocities (and obviously precipitations) are reduced.

5.2 Swiss case

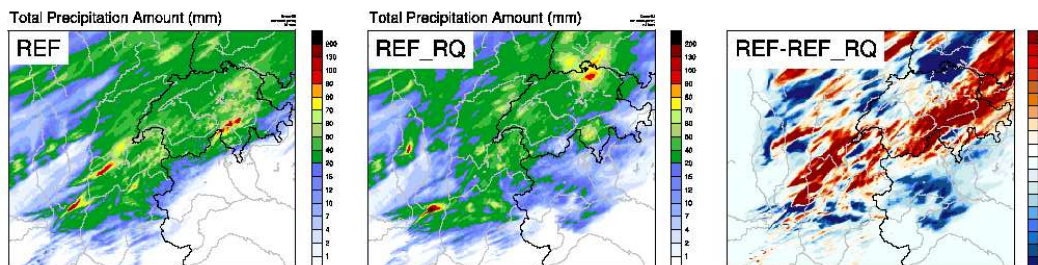
The most evident feature of the LHN run REF_R (panel b of fig: 5.9) is the artificially looking structure in the southwestern border of the SRN domain. Infact, the SRN quality is close to zero in this area due to a visibility cone of the La Dole radar and to a progressive range effect. The model analysis simulated significant precipitation in this area which the LHN sucessfully reduced. Just outside the SRN domain, on the other hand, there are precipitation bands along the border. Again, these are compatible with the mechanism proposed in Fig. 5.4. The quality function, panel c fig: 5.9, recognizes this as an area in which the radar data should not have a strong impact on the model. Accordingly, the run with the quality function REF_RQ strongly reduces the artifacts, both within the radar domain and just across its border. On the rest of the SRN domain the quality function has a minor impact on the LHN scheme, as the model did not produce precipitation in areas of low radar data quality.



(a) REF-REF_R



(b) REF_R-REF_RQ



(c) REF-REF_RQ

Figure 5.9: 48h accumulation

Chapter 6

Summary and discussion

With the rapid increase in the last few years of the resolution of NWP, the need for data that trace the initial state of the atmosphere is greater and greater. Problems arise in providing these data and in the way we can combine them seeing that they came from a very different ensemble of instruments.

So, assimilation of data, the statistical discipline which aims to combine all the initial conditions information, is a very underdeveloped field.

Radar observations, via their great resolution and frequency, can be instrumental in this field. Obviously it is absolutely necessary to know radar data quality and take this into account during the assimilation.

This thesis work concerned both the impact of radar data assimilation in high-resolution models and how understand and improve the quality of this measurement.

6.1 Impact of radar data quality function

In this contribution a new, yet simple, empirical quality description of radar-derived quantitative precipitation estimates (QPE) was proposed. It was constructed using a long-term frequency of occurrence of precipitation analysis. Hereby frequent (rare) occurrence of precipitation is assessed as 'good' ('bad') quality, while rest clutter was identified and assigned quality zero. How and for what frequencies the quality decreases from one to zero is tunable to some extent, and can be conceived as an overall weight one subjectively intends to assign to the radar observation. The empirical radar data quality function proposed with a moving 90-day accumulation window has the following characteristics:

- it is conceptually simple and easy to construct;

- it reproduces the main error structures and is, therefore, a plausible way to account for the average problems in radar QPE;
- it has a sufficiently smooth day-to-day evolution for an Alpine climate;
- it accounts for the seasonal variability of the radar QPE;
- it is, to some extent, generic, in that it can 'easily' be evaluated for different radar networks (here for two) and, potentially, also for heterogeneous networks in that it does not rely on specifics of the radar processing.

The impact of the proposed quality function on the LHN assimilation has been found to be beneficial since:

- it reduces artifacts which can be induced close to boundaries of the radar domain;
- it represents an additional means to reduce rest clutter and its potentially harmful impact on the analysis;
- it does not artificially interfere with the model precipitation in areas where the radar quality is sub-optimal;

The limitations of such an empirical radar data quality description are recognized in that:

- it is empirical and not physically based and does, therefore, describe the effects of the error sources without explicitly taking them into account;
- it is an average, rather than an instantaneous quality description and thus accounts for average errors, rather than actual real time errors;
- the present formulation will yield good (bad) quality in case of precipitation occurrence much higher (lower) than climatology, hence not reflecting effective radar data quality;
- the quality is described as a weight between 0 and 1, i.e. an index, rather than in units of the precipitation, and it is, therefore, not directly applicable to statistical data assimilation schemes as ensemble Kalman filters, for instance, nor does it, in its present form, account for error covariances.

In a radar network single radars may be missing occasionally, or for longer periods, a fact which is not easily accounted for in the presented approach. A solution for this problem could be performing the analysis on the single radars and , with the composite procedure of the network, producing the radar data quality function. Alternatively, the quality information thus obtained could be used in support of the compositing method, choosing the radar with the best quality for a given pixel.

An obvious extension of this work is to apply the quality function to longer assimilation periods and assess its impact more systematically. Also, its impact on the free forecasts has yet to be addressed. In view of the OPERA efforts to make radar data available on a European scale this approach could be a candidate method to pragmatically deal with the inevitably very heterogeneous radar data quality in the framework of assimilation methods like LHN.

6.2 Impact of radar rainfall assimilation

Radar rainfall assimilation via Latent Heat Nudging scheme in the COSMO-2 model is a research field that has seen great effort spent in this last year by Rossa and Leuenberger.

His possible impact on operative use, like hydrological alert, can be a very important feature From this point of view the choice of the Mestre flood has been absolutely correct.

The main relevant impact of radar data assimilation via LHN scheme can be resumed in:

- the radar QPE assimilation has a very large impact on the simulation in analysis mode in that it features a very efficient drying of the excess of precipitation and excellent triggering of the observed convection
- there is a clear response of the low level wind and convergence field illustrating that the LHN method is able to modify the microscale circulation
- the positive impact of the LHN in analysis mode is carried over in the free forecast mode for 2-3 hours; after this time the 'wrong' upper-level dynamics takes over and re-introduces the incorrect precipitation system; this clearly pinpoints the limitation of the LHN scheme to substantially modify the mesoscale circulation, especially at upper levels.

In the perspective of a rapid update cycle (update forecast every, say, 3 hours) LHN scheme brings about an improvement of the QPF on a timescale

comparable to the lifetime of organized convection. The results highlight a large potential for improving hydrological forecasting, especially for heavy convective precipitation events.

Bibliography

- M. Berenguer and I. Zawadzki. A study of the error covariance matrix of radar rainfall estimates in stratiform rain. *Weather and forecasting*, 2008.
- J. William Conway, Chip Barerre, Gabriele Formentini, Luciano Lago, Andrea Rossa, and Michela Calza. Flash flood prediction in italy: Development and testing of a new capability. In *Proceedings of 21st Conference on Hydrology*. AMS Annual, AMS, January 2007. URL <http://ams.confex.com/ams/pdfpapers/121128.pdf>.
- G. Doms and U. Schättler. A description of the nonhydrostatic regional model LM: Part I: Dynamics and numerics. available from <http://cosmo-model.org>, 2002.
- A. Fornasiero, P. P. Alberoni, R. Amorati, and C. Marsigli. Improving the radar data mosaicking procedure by means of a quality descriptor. In *ERAD Publication Series*, volume 3, pages 378–341, 2006.
- K. Friedrich and M. Hagen. Wind Synthesis and Quality Control of Multiple-Doppler-Derived Horizontal Wind Fields. *Journal of Applied Meteorology*, 43:38–57, 2004. URL .
- G. A. Gal-Ghen and C. J. Sommerville. On the use of a coordinate transform for the solution of the navier-stokes equations. *J. Comput. Phys.*, 1975.
- Germann and Joss. Operational measurement of precipitation in mountainous terrain. In *Weather Radar: Principles and advanced applications*, P. Meischner, Springer Series, Physics of Earth and Space Environments: 52–75, 2004a.
- G. Galli M. Boscacci M. Bolliger Germann, U. and M. Gabella. Quantitative precipitation estimation in the alps: where do we stand? *ERAD Publication Series*, 2:2–6, 2004.

- U. Germann and J. Joss. *Weather Radar: Principles and Advanced Applications*, edited by P. Meischner in Springer monograph series 'Physics of Earth and Space Environment', hardcover Operational measurement of precipitation in mountainous terrain, page 337pp. Physics of Earth and Space Environment. Springer, 2004b.
- U. Germann, G. Galli, M. Boscacci, and M. Bolliger. Radar precipitation measurement in a mountainous region. *Quarterly Journal of the Royal Meteorological Society*, 132:1669–1692, 2006.
- J.J. Gourley, J. Zhang, R. A. Maddox, C. M. Calvert, and K. Howard. A real-time precipitation monitoring algorithm - quantitative precipitation estimation and segregation using multiple sensors (qpe-sums). In *Preprints, Symp. On Precipitation Extremes: Predictions, Impacts, and Responses.*, pages 57–60. AMS, AMS, 2001. Albuquerque, NM.
- I. Holleman, D. Michelson, G. Galli, U. Germann, and M. Peura. Quality information for radars and radar data (opera document available at <http://www.knmi.nl/opera>). EUMETNET OPERA document, 2006. URL www.opera.nl.
- C. D. Jones and B. Macpherson. A latent heat nudging scheme for the assimilation of precipitation data into an operational mesoscale model. *Meteorol. Appl.*, 4:269–277, 1997. URL .
- J. et al. Joss. Operational use of radar for precipitation measurements in switzerland. Technical report, NRP 31, vdf Hochschulverlag an der ETH Zuerich, 108 pp., ISBN 3 7281 2501 6, 1998.
- E. Kalnay. Atmosphere modelling, data assimilation and predictability. *Cambridge university press*, 2003.
- R. J. Keeler and S. M. Ellis. Observational error covariance matrices for radar data assimilation. *Physics and Chemistry of the Earth, Part B: Hydrology, Oceans and Atmosphere*, 25(10-12):1277 – 1280, 2000. ISSN 1464-1909. doi: DOI: 10.1016/S1464-1909(00)00193-3. URL <http://www.sciencedirect.com/science/article/B6VPV-41F63DT-35/2/3f139a35a6a> First European Conference on Radar Meteorology.
- D. Leuenberger and A. Rossa. Revisiting the latent heat nudging scheme for rainfall assimilation of a simulated convective storm. *Meteorology and Atmospheric Physics*, available online:25pp, 2007.

- B. Macpherson, M. Lindskog, V. Ducrocq, M. Nuret, G. Gregoric, A. M. Rossa, G. Haase, I. Holleman, and P. P. Alberoni. Quality and assimilation of radar data for nwp. In *Weather Radar: Principles and advanced applications*, P. Meischner, Springer Series, Physics of Earth and Space Environments:255–279, 2004.
- D. Michelson, T. Einfalt, I. Holleman, U. Gjertsen, K. Friedrich, G. Haase, M. Lindskog, and J. Szturc. Weather Radar Data Quality in Europe: Quality Control and Characterization. *ERAD-3, Visby, Sweden, 6-10 September 2004*, 2004. URL .
- A.. Rossa and D. Leuenbeger. Sensitivity of the lhn scheme to non-rain echoes. *Meteorological Applications*, 15:503–511, 2008.
- M. Bruen M.D. Fruehwald Macpherson B. Holleman I. Michelson D. Rossa, A.. and s. Michaelides. Cost 717 action . use of radar observation in hydrology and nwp models. *Cost Meteorology*, page 286, 2005.
- C. H. Schraff. Mesoscale data assimilation and prediction of low stratus in the alpine region. *Meteor. Atmos. Phys.*, pages 21–51, 1997.
- D. Sempere-Torres, G. Pegram, X. Llorc, C. Velasco-Forero, and M. Franco. "real-time assessment of accuracy and quality in quantitative precipitation estimation. In *Proceedings of Fifth European Conference on Radar in Meteorology and Hydrology (ERAD2008). Helsinki (Finlandia). ISSN: 978-951-697-676-4.*, volume 4 of *ERAD Publication Series*, 2008.
- K. Stephan, S. Klink, and C. Schraff. Assimilation of radar-derived rain rates into the convective-scale model cosmo-de at dwd. *Quarterly Journal of the Royal Meteorological Society*, 134(634):1315–1326, 2008. URL <http://dx.doi.org/10.1002/qj.269>.
- J. Steppeler, G. Doms, U. Schättler, H.-W. Bitzer, A. Gassmann, U. Damrath, and G. Gregoric. Meso-gamma scale forecasts using the nonhydrostatic model LM. 82:75–96, 2003.